JOURNAL OF GEOPHYSICAL RESEARCH, VOL. 113, D21208, doi:10.1029/2008JD010272, 2008

Aerosol characterization during the summer monsoon period over a tropical coastal Indian station, Visakhapatnam

B. L. Madhavan,[1] K. Niranjan,[1] V. Sreekanth,[2] M. M. Sarin,[3] and A. K. Sudheer[3]

Received 14 April 2008; revised 25 June 2008; accepted 4 August 2008; published 14 November 2008.

[1] Columnar optical depth and near-surface mass concentration of aerosols over Visakhapatnam, an urban location along the east coast of India during the summer monsoon period (May–August 2005), were measured simultaneously along with chemical sampling for water-soluble ionic species (NH_4^+, Na^+, K^+, Mg^{2+}, Ca^{2+}, Cl^-, NO_3^-, SO_4^{2-}, and HCO_3^-). The mean aerosol optical depth (AOD) (0.5 μm) and Angstrom parameters (α, β) during this period were obtained as 0.72 ± 0.39 and 0.88 ± 0.39, 0.48 ± 0.36, respectively. The total surface aerosol mass concentration varied from 95 to 128 ($\mu g/m^3$), out of which coarse mode dominated by 45%. While Cl^-, Na^+, K^+, and Mg^{2+} (sea salts) contributed nearly 56%, SO_4^{2-} and NO_3^- (anthropogenic constituents) contributed 33% in surface aerosol constituents. During this period, high spectral variability in AOD, negative curvature of second-order Angstrom coefficient (α^1), abundance of columnar submicron aerosols, role of air mass trajectories as tracers of long-range transport, cation deficiency, and sea-salt dependence on wind speed are some of the observations over Visakhapatnam. The synergy of the results from these complementary measurements can be reflected while computing the aerosol radiative forcing.

Citation: Madhavan, B. L., K. Niranjan, V. Sreekanth, M. M. Sarin, and A. K. Sudheer (2008), Aerosol characterization during the summer monsoon period over a tropical coastal Indian station, Visakhapatnam, *J. Geophys. Res.*, *113*, D21208, doi:10.1029/2008JD010272.

1. Introduction

[2] Atmospheric aerosols produced by both natural and anthropogenic processes are major players within Earth's climate system [*Intergovernmental Panel on Climate Change* (*IPCC*), 2001] affecting the radiation budget, cloud processes and surface air quality. As their life time is of the order of days, aerosols are inhomogeneous in time and in space, with much higher concentrations near the sources and hence are predominantly regionally distributed. Different particle origins result in mixture of chemical species with different optical properties [*d'Almeida et al.*, 1991]. These have strong bearing on the seasonal variation of the solar heating of the surface, prevailing circulations and related boundary layer processes which influence transfer of flux from the higher regions to lower levels of the atmosphere and vice versa [*Stull*, 1988]. Aerosol physical properties at a given location are largely governed by the local processes that lead to aerosol formation, which are modified by the prevailing meteorology, besides transport of aerosols from sources of nonlocal origin. Marine aerosols produced in the surf zone at high concentrations are immediately available for heterogeneous chemical reactions and influence the composition of aerosols at coastal locations [*Vignati et al.*, 2001]. *Zhang et al.* [1993] reported that aerosol chemical composition, particle size distribution and air mass back trajectories can serve as tracers for the origin of the air mass sampled.

[3] Size distribution and chemical composition of aerosols are most important properties as far direct and indirect radiative effects are concerned [*IPCC*, 2001]. Near-surface aerosol contribution to the columnar abundance is significant when the transport process becomes trivial. Thus while estimating the radiative impact of aerosols, the link between the properties of near-surface aerosols and columnar spectral optical depths needs to be understood. Over the Indian landmass, studies focusing on the spatial heterogeneity of aerosol properties during premonsoon and monsoon season are scarce. However, such data are essential to assess the complex response of the hydrological cycle to regional aerosol radiative forcing and also to delineate the temporal changes. Direct and indirect aerosol effects are largely influenced by ambient RH, aerosol water solubility and chemical composition of the water-soluble material. Water-soluble aerosol compounds, such as ammonium (NH_4^+), nitrate (NO_3^-), chloride (Cl^-) and sulphate (SO_4^{2-}) play a major role in the nucleation and growth of cloud droplets [*Roberts et al.*, 2002].

[4] As atmospheric aerosols are highly heterogeneous and poly dispersive in nature, no single technique or group of techniques is adequate for entire characterization of atmospheric aerosol properties over the extremely wide

[1]Department of Physics, Andhra University, Visakhapatnam, India.
[2]Space Physics Laboratory, Vikram Sarabhai Space Centre, Thiruvananthapuram, India.
[3]Physical Research Laboratory, Ahmedabad, India.

0148-0227/08/2008JD010272$09.00

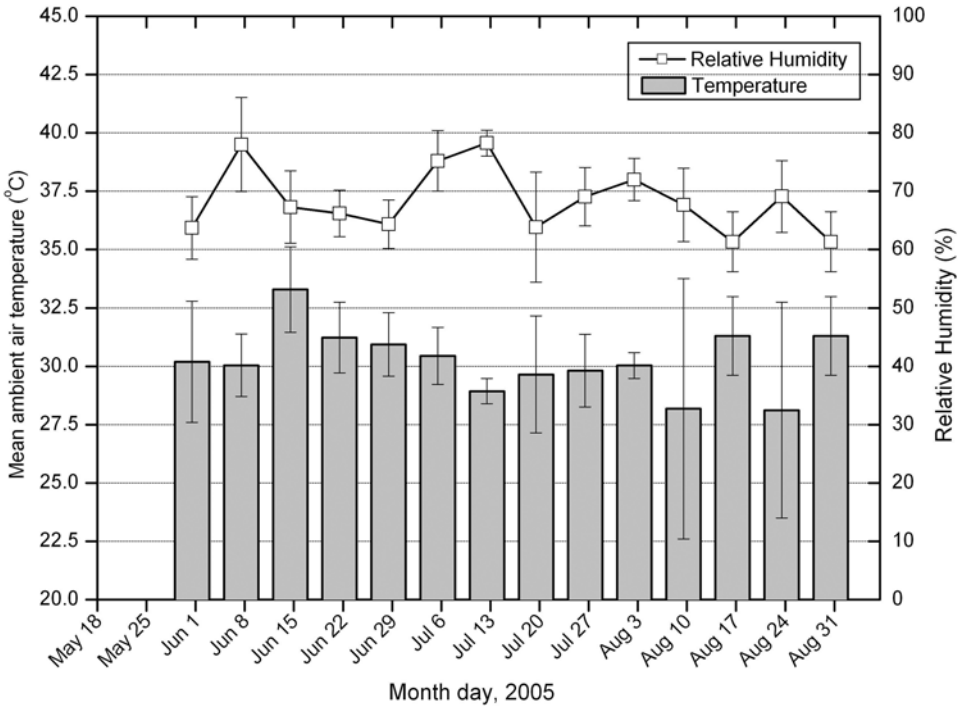

Figure 1. Temporal variation of surface meteorological parameters (mean ambient air temperature and relative humidity) measured over VSP during summer monsoon season (May–August 2005).

range of particle size, shape and chemical composition. The aerosol characteristics measured at the surface and in a column have been found to be different owing to (1) variations in the source regions from where the aerosols are transported to the measurement location at different heights [*Franke et al.*, 2003], (2) altitudinal differences in physical and chemical compositions [*Slater and Dibb*, 2004] and (3) differences in the contribution of the boundary layer aerosols to the column [*Franke et al.*, 2003; *Smirnov et al.*, 2000]. The selection of a particular method depends primarily on the type of application. In the case of atmospheric aerosols, the size distribution and mass concentration are vital to understand their source strength and environmental impact; the aerosol optical thickness is primary for determining the optical properties; while chemical composition along with all the prementioned parameters give a clear understanding about radiative effects and climatic implications.

[5] The surface-level characteristics can be quite different compared to the columnar values as different types of aerosols vary depending on their scale heights. *Niranjan et al.* [2004] reported the formation of new types of aerosols with completely different physical properties owing to mixing of the two different air masses, namely, continental and maritime indicating that the properties of aerosols are strongly dependent on the air mass history in a coastal environment and are a complicated mixture of marine, anthropogenic and rural aerosols [*Moorthy et al.*, 1991, 1993; *Vignati et al.*, 2001].

[6] In this paper, we report some interesting findings from simultaneously measured aerosol physical, chemical and optical parameters observed during the summer monsoon period (May–August 2005) over Visakhapatnam, an urban coastal location over east coast of India. The aerosol parameters include aerosol optical depth, Angstrom parameters, near-surface aerosol mass concentration and water-soluble aerosol ionic species.

2. Site Description and Prevailing Meteorology

[7] Measurements were carried out at the Department of Physics, Andhra University, Visakhapatnam (17.7°N, 83.3°E; 230 m asl) which is very close to the Bay of Bengal sea coast (~500 m away) and is subjected to the sea breeze activity on all days. Visakhapatnam (VSP) is an industrialized urban coastal location on the east coast of India with an industrial area in the southwest. The mixing region aerosols dispersed by the convection motion during the daytime remain there even after the sunset for about 4–6 h [*Delage*, 1974]. Thus, the effect of wind speed on mixing region aerosol number density is rather complex, and the effect of local wind and wind speed history are strongly coupled [*Gathman*, 1983]. During the winter season the winds are north-northeasterly while during the summer they are southwesterly. The station experiences two spells of rainfall: the southwest monsoon (June–August) and the northeast monsoon (October and November). The wind predominantly coming from the southwest (SW) direction carries sufficient moisture to give the summer monsoon rain to almost all parts of India [*Rao*, 1976], though geographical variation does exist in the rainfall distribution [*Sikka*, 1980]. Meteorological data used in the present study are obtained from the digital hygrothermometer (relative humidity and temperature of ambient air) and from the radiosonde data of Visakhapatnam (station code: 43150) available in the University of Wyoming website (www.weather.uwyo.edu/upperair/sounding.html), the surface-level wind speed and wind direction were obtained. Figure 1 shows the average values of ambient air

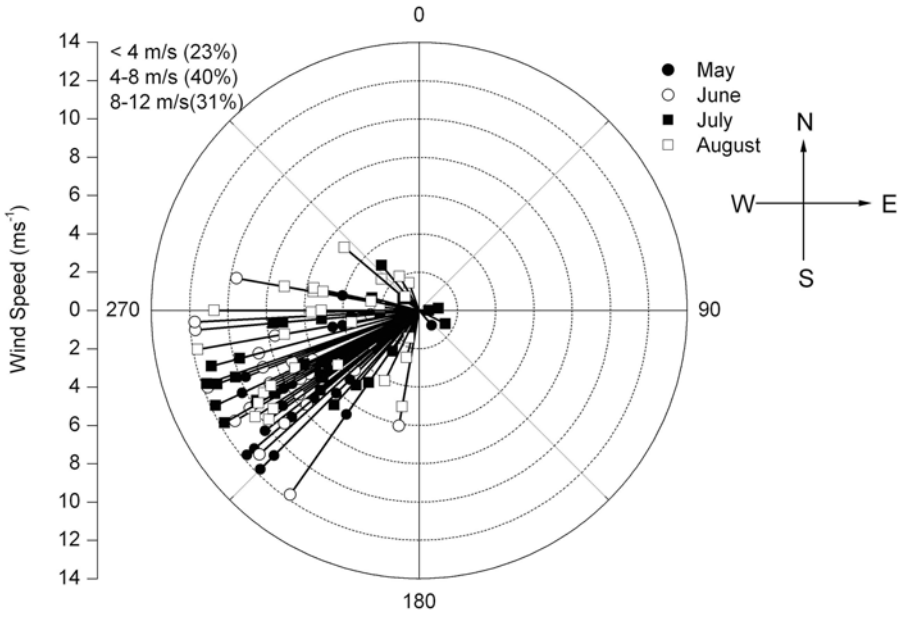

Figure 2. Daily average values of surface-level wind speed (ms^{-1}) and wind direction (degrees) measured over Visakhapatnam during summer monsoon season (May–August 2005).

temperature and relative humidity (RH) for the period of daytime aerosol measurements made during May–August 2005. The surface air temperature is in general high with (30 ± 4) °C, while the relative humidity varied in the range of (70 ± 12)% during the daytime of measurements. The NCEP data of May–August 2005 also showed that the surface-level wind (at 850 hPa) was generally from west and southwest direction with mean wind speed ranging from (7.6 ± 3.9) ms^{-1}. Figure 2 shows the wind speed and wind direction prevailed over Visakhapatnam during May–August 2005. During this period, the prevailing wind is southwesterly and the aerosols over Visakhapatnam will have a possible influence of marine air masses reaching this region from Arabian Sea in the south via Indian subcontinent, besides contribution from local sea spray aerosols. The high speeds also facilitate rapid transport of nascent continental aerosols leading to the formation of new submicron aerosols over the oceanic environment (which provides ample RH) through secondary (gas to particle) production.

[8] In the present work, the data considered was from 18 May to 31 August 2005. The Indian summer monsoon is a part of a large-scale circulation pattern which develops in response to the thermal gradients between the warm Asian continent in the north and cooler Indian Ocean in the south. A strong southwesterly flow in the lower troposphere brings a substantial supply of moisture into India which is released as precipitation almost across the entire country. Monsoon and aerosol loading in the atmosphere are very intricately related to each other because amount and type of aerosols which act as cloud condensation nuclei (CCN) together with available moisture in the atmosphere decides the amount of rainfall that occurs over the region. Though establishing a relationship between aerosol loading in the atmosphere and monsoon prediction in the region is beyond the scope of the present work, aerosol characterization during the monsoon period can throw light on the role of aerosols on frequent/deficient rainfall over the region.

3. Instrumentation and Measurements

[9] A list of instruments used at VSP and the specification of data availability on the dates of simultaneous operation are presented in Table 1. A handheld 5-channel MICROTOPS II Sun photometer (Solar Light Co., USA, purchased in January 2004) [*Morys et al.*, 2001] was used for measuring Aerosol Optical Depth (AOD) simultaneously at five wavelength bands centered around 0.38, 0.44, 0.5, 0.675 and 0.87 μm. Field of view of each collimator is about 2.5° and full width half-maximum (FWHM) bandwidth of all filters lie in the range of 3 to 10 nm. The AOD values at the respective wavelengths are measured at half hourly interval from 0700 to 1700 local time (LT) on cloud free time during the days of observation. The overall error [*Russell et al.*, 1993] in the aerosol optical depth can be due to: (1) diffuse radiation entering the optical channel, (2) computation error in relative air mass (a geometric term to account for relative increase in optical path length as solar zenith angle increases), (3) deviation of the calibration coefficient with time and (4) error associated with the uncertainty in the optical depths owing to Rayleigh scattering and absorption by O_3, NO_2 and water vapor. The combined error in the estimated AOD owing to all the above mentioned errors is in the range of 0.009 to 0.011 at different wavelengths (which is 2% to 10% of the AOD). The absolute uncertainty in the AOD values is less than 0.03 at all wavelengths. The typical agreement between multiple MICROTOPS II instruments is within 1–2%. Also, the measurements through broken clouds or in very hazy conditions show variability of 1–2%.

[10] Near-surface, size-segregated, total aerosol mass concentrations ($\mu g\ m^{-3}$) were measured using the Quartz Crystal Microbalance (QCM) cascade impactor (model

Table 1. Data Availability From Various Aerosol Instruments[a]

Date	AOD	QCM	HVS	RH and Temperature
18 May 2005	na	na	a	na
25 May 2005	na	na	a	na
1 June 2005	a	a	a	a
8 June 2005	a	na	a	a
15 June 2005	a	a	a	a
22 June 2005	a	a	a	a
6 July 2005	na	a	a	a
13 July 2005	a	a	a	a
20 July 2005	na	a	a	a
27 July 2005	a	na	a	a
10 Aug. 2005	a	a	a	a
17 Aug. 2005	a	a	a	a
24 Aug. 2005	a	a	a	a
31 Aug. 2005	a	a	a	a

[a]Abbreviations are as follows: a, available; na, not available.

PC-2, California Measurements Inc., USA), which provides real time measurements in 10 size bins, with 50% cut off diameters namely, >25 μm, 12.5, 6.4, 3.2, 1.6, 0.8, 0.4, 0.2, 0.1 and 0.05 μm for the stages 1 to 10, respectively. The 50% cut off of each stage is given in terms of particle diameters from the aerodynamic diameter taking the particle density as 2 μg cm^{-3}. The density of aerosols is reported to vary from 1.8 to 3.0 μg cm^{-3} from maritime to urban locations [*Hanel*, 1976; *Pruppacher and Klett*, 1978] and as such the value used here is well with in the range. Its pump aspirates the ambient air at a flow rate of 0.24 L min^{-1}. The optimum sampling time is taken as that time which is sufficient to impart a frequency change of 20 to 30 Hz with a tolerance of −5 to +10 Hz. So, the typical sampling duration was kept as 5 min. Measurements were restricted to periods when the ambient RH was less than 80%. Following the error budgeting given by *Pillai and Moorthy* [2001], the error in the estimated mass concentration was in the range of 10 to 15% for each measurement. Higher chances of error in the mass measurement for all stages of QCM occurs under high relative humidity conditions during monsoon season because within a measurement time of 5 to 10 min, there could be an evaporation loss of the adsorbed water from the water-soluble particles which are being collected under low-pressure conditions inside the impactor stages [*Ganguly et al.*, 2006] and therefore we have avoided measurements above 80% humidity levels.

[11] A high-volume sampler (HVS, ENVIROTECH'S Model APM-430) of Physical Research Laboratory (PRL), Ahmedabad was installed for chemical characterization over the location. The air borne particulates are passed through a high efficiency filter paper (Pal Gelman or Whatman) at a high flow rate of 1.1 to 1.7 m^3 min^{-1}, which retains the particles. Here high volumes of air are drawn through fiber filters. The mass concentration of total suspended particulate matter (TSP) in ambient air, expressed in μg m^{-3}, is calculated by measuring the mass of collected particulates and the high volume of air sampled.

[12] On average, an aerosol sample was collected every 8th day over VSP (mostly on every Wednesday of the week). A total of 14 samples were collected during May–August 2005 at VSP. The samples collected were taken to PRL, Ahmedabad for chemical analyses. The procedure suggested by *Rastogi and Sarin* [2005] was adopted for obtaining the water-soluble constituents (NH_4^+, Na^+, K^+, Mg^{2+}, Ca^{2+}, Cl^-, NO_3^-, SO_4^{2-} and HCO_3^-). The precision estimated from the standard deviation of repeat measurements of standards and samples, was better than 4% for Cl^-, NO_3^- and SO_4^{2-}; 2% for HCO_3^-, Na^+, K^+ and NH_4^+; and 5% for Ca^{2+} and Mg^{2+}. Only water-soluble constituents were analyzed because of their hygroscopic significance during the summer monsoon period. Under stable sea breeze conditions, simultaneous diurnal measurements using all the three instruments were made regularly on every eighth day (i.e., on Wednesday) during the period of study.

4. Results and Discussion

4.1. Aerosol Optical Depth and Angstrom Parameters

[13] Aerosol optical depth (τ_λ) at a given wavelength λ depends upon the amount, size distribution and chemical composition of aerosols which can readily be used to estimate the aerosol radiative forcing. Sun photometer measured spectral aerosol optical depths on each day were averaged to get the daily mean AOD. The AOD in the visible region of the solar spectrum is more important to the radiative forcing and is determined mainly by the amount of nucleation and accumulation mode particles. An estimate of the relative dominance of sub micron aerosols was obtained by estimating the Angstrom wavelength exponent α in the relation [*Angstrom*, 1964]: $\tau_\lambda = \beta\lambda^{-\alpha}$, where τ_λ are the spectral AOD, λ is the wavelength in μm and β the turbidity coefficient (equivalent to AOD at 1 μm). Although α and β are assumed independent of the wavelength, it is well known that both parameters depend on wavelength. α and β have been estimated for each of the observed AOD spectra by evolving a linear least squares fit to Angstrom relation in a log-log scale and are averaged daily. In general, the fits were very good with a correlation exceeding 0.95.

[14] The temporal variation of daily mean AOD at 0.5 μm and Angstrom coefficients (α and β) measured during the study period (June–August 2005) are shown in Figure 3. Vertical lines on the top of each corresponding symbol indicate $\pm 1\sigma$ variation about the mean values measured during the day. In general, the AOD (0.5 μm) values varied from 0.29 to 1.11 with a mean at 0.72 ± 0.39, while the values of α were in the range ~0.35–1.39 with a mean value of 0.88 ± 0.39 and those of β were in the range 0.15–1.15 with a mean of 0.48 ± 0.36. Variation in the α values during the summer monsoon period indicates high spectral variability in AOD. Decrease in α can occur either because of a relative decrease in number of smaller sized particles with respect to larger ones or because of an increase in coarser particles in the atmospheric column. As the smaller particles over continental locations are primarily produced by anthropogenic activities, the value of α can be considered as a measure of anthropogenic influence [*Moorthy and Satheesh*, 2000]. An interesting observation is that the temporal variation of α was almost opposite in nature to that of the AOD at 0.5 μm. Higher values of AOD were associated with lower values of α and vice versa, indicating that the increase in AOD is mainly due to the presence of coarse mode aerosols (particles of size >1 μm). The coarse aerosols observed commonly over the oceanic regions are either sea salt produced in situ by the winds or the transported mineral dust [*Prospero*, 1979]. This is further corroborated by the variation of β shown in open circles in

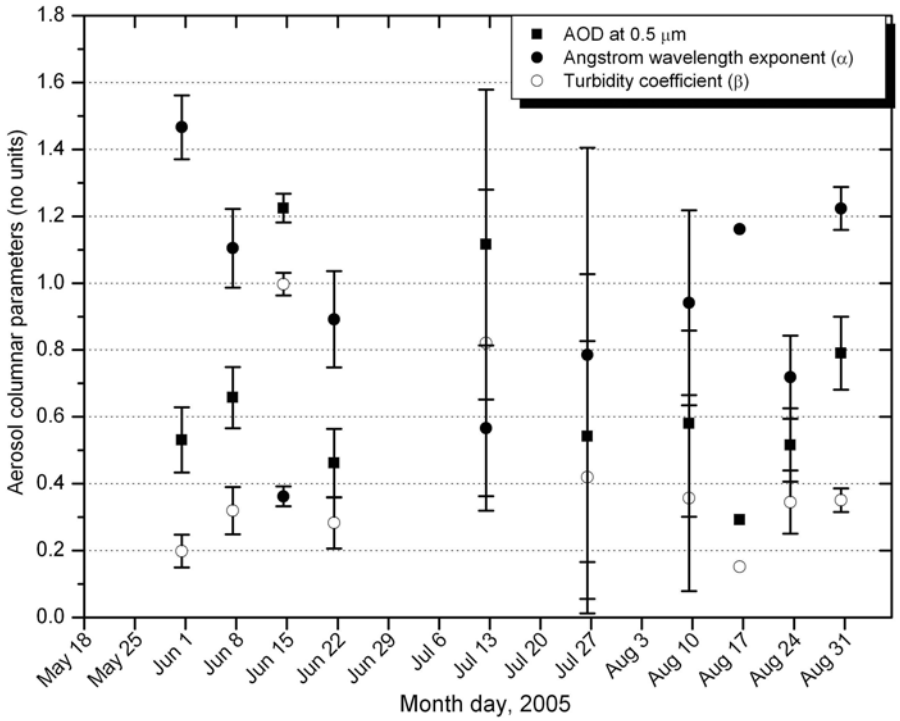

Figure 3. Time series of average values of AOD at 0.5 μm measured during the days of observation with the variation of Angstrom wavelength exponent α and Angstrom turbidity coefficient β estimated from the daily mean AOD spectra.

Figure 3, the variations of which are quite similar to that of AOD. Since the surface wind speeds were generally high (>5 ms^{-1}) and showed some significant increases around the periods of higher AOD, it is likely that the sea spray production mechanisms by prevailing winds might have been partially responsible for the increase in AOD or β though it may not account for such larger increase (Figure 3). Further *Niranjan et al.* [2007] from micropulse lidar observation of aerosol vertical distribution reported that during events of air mass flow from Arabia/central India, elevated aerosol layers with significant fraction of dust were observed during premonsoon period, which might have contributed to the increase in AOD with simultaneous decrease in α.

[15] The spectral variation of AOD clearly showed that at shorter wavelengths AOD are higher while at longer wavelengths they are relatively lower. This trend is observed for all days irrespective of the sky condition. Figure 4 shows the AOD spectrum for four representative days of the observation period, namely, 1 June, 13 July, and 10 and 31 August, comprising high AOD arising out of different air mass regimes. It is observed that AODs at almost all wavelength channels were higher during the four days (or during monsoon season). Comparing the AOD spectra for 1 June and 13 July, we find that although AOD values at all wavelength channels are higher, this increase is not spectrally uniform, and rather percentage increase in longer wavelengths AOD is larger (~260%) than at shorter wavelength channels (~72%). Comparison of the AOD spectra for 1 June and 10 August, negligible difference in AOD value is found below 0.44 μm but at longer wavelengths (i.e., at 0.87 μm) AOD on 10 August is higher than on 1 June by nearly 68%. Both these observations show that 10 August is characterized by increased levels of coarse mode aerosols in the atmosphere and hence the AOD measurements in the higher wavelengths are more affected. Next comparing the AOD spectra of 1 June with that of 31 August, we find that the AOD spectrum is almost uniform between 0.38 to 0.5 μm but there is a slight increase (~20–40%) in the shorter wavelengths AOD indicating the raise in the submicron aerosol concentrations. Though, it is observed that both 13 July and 10 August resembled the similar uniform spectral variation, there is an enhancement by 1.8 times the spectral AOD values of the former than those on 10 August.

[16] The Angstrom exponent (α) itself varies with wavelength, and a more precise empirical relationship between aerosol extinction and wavelength is obtained with a second-order polynomial fit [*Schuster et al.*, 2006; *Kaskaoutis and Kambezidis*, 2006]: $\ln \tau_\lambda = a_o + \alpha \ln \lambda + \alpha^1 (\ln \lambda)^2$, where the coefficient α^1 accounts for a curvature often observed in Sun photometry measurements. The second derivative is a measure of the rate of change of slope with respect to wavelength. The curvature can be an indicator of the aerosol particle size, with negative curvature indicating aerosol size distributions dominated by the fine-mode and positive curvature indicating size distributions with a significant contribution by the coarse mode [*Schuster et al.*, 2006]. Evaluating the second-order Angstrom coefficient α^1 to our AOD measurements at 0.38, 0.5 and 0.87 μm, it varied between -18 to 2 with a mean at -9.2 ± 5.0. It is observed that the positive curvatures of α^1 dominated during the prerainy days while the negative curvatures of α^1 dominated the postrainy days indicating that the coarse mode aerosols were wet deposited while the fine-mode aerosols act as surfaces for CCN. These fine-mode aerosols undergo transformation processes between a postrainy day to a prerainy day.

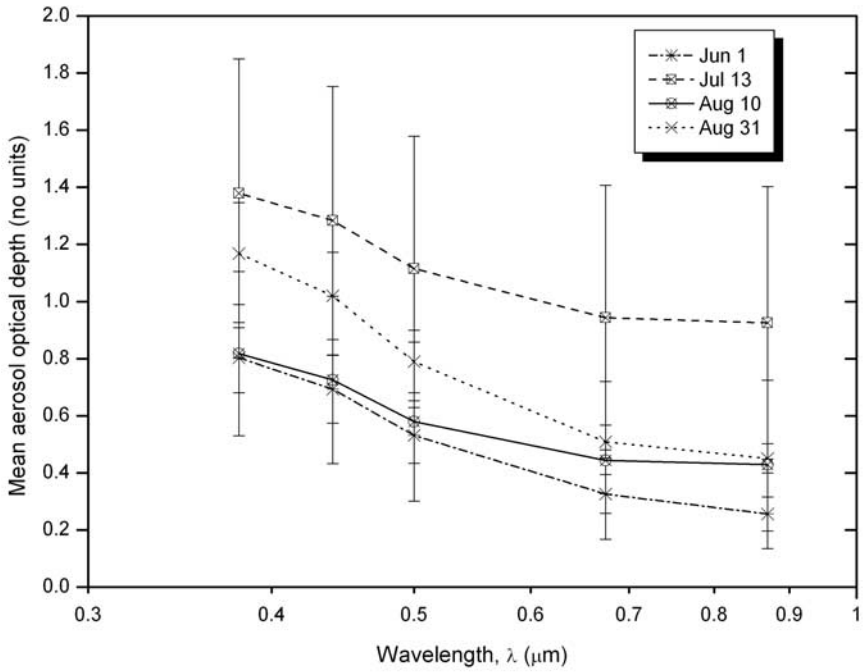

Figure 4. Spectral AOD variation for four representative days during the period of summer monsoon season (May–August 2005).

[17] Although summer monsoon spans from June to August over Visakhapatnam, a decrease in AOD values owing to wet removal of aerosols can be expected during rain events. However, this decrease does not seem to be always taking place primarily because even during monsoon, rainfall is unevenly distributed over the entire season as it occurs in certain spells with large intermittent gaps. The abundance of submicron (accumulation) aerosols, which offer large surface area for scattering of radiation, during the monsoon period (June–August) might have resulted in higher spectral optical depths.

4.2. Air Mass Trajectories and Possible Transport Pathways

[18] Earlier studies on the effect of changes in wind speed on aerosol characteristics have indicated a significant increase in AOD [*Smirnov et al.*, 1994; *Moorthy et al.*, 1997], surface aerosol concentration [*O'Dowd and Smith*, 1993] and mass loading [*Exton et al.*, 1985] with increase in wind speed. *Exton et al.* [1985] also reported that the effect appears to be stronger at larger sizes. Aerosol properties over coastal oceanic regions would be significantly modified by the advection of aerosols from the adjoining landmasses under favorable wind conditions and vice versa. With a view to examine the effect of air mass trajectories, which act as potential conduits for aerosol transport, using HYSPLIT (HYbrid Single Particle Lagrangian Integrated Trajectory) model of NOAA (www.arl.noaa.gov/ready/hysplit4.html), seven day back trajectories for all days during the period of study were computed. Although surface-level wind flow is predominantly southwesterly, transport of dust aerosols from distinct regions of west Asia and northern Africa to this region continue to occur at high altitudes during this season. *Niranjan et al.* [2007] have shown the presence of high-altitude aerosol layers above the boundary layer in the height region between 1.6 to 5 km during summer months of March–May 2005, which indicated an increase in AOD at 0.5 μm by 0.05 to 0.25 during the presence of such layers while there were no signs of existence of proportional increase in the surface aerosol mass concentrations. In Figures 5a and 5b, the backward trajectories of the air mass at 500, 1500 and 2500 m altitude calculated using the FNL data of NOAA HYSPLIT model for 1 June ($1.4 < \alpha < 1.5$; high) and 13 July ($0.5 < \alpha < 0.6$; very low) show that the air mass at surface level continues to prevail from Arabian Sea/Indian Ocean in all days of observation while at high altitudes above 1 km (i.e., at 1500 and 2500 m) there were respective tracers of possible transport from central/northern parts of India and from the Arabian/African countries. Analysis of the vertical velocity profiles along the trajectory predicted by HYSPLIT indicated that: (1) in both the cases, the air parcel ending at 500 m (red trajectory) originated at almost the same altitude and the path remained at the surface level; (2) in Figure 5a, all the air parcels ending at 500, 1500 (blue trajectory) and 2500 (light green trajectory) meter altitude were of surface origin which experienced strong downward and upward vertical velocities during their course of their ascent; (3) in Figure 5b, the air parcels ending at 1500 and 2500 m respectively experienced strong upward vertical velocities during 11 to 13 July. The mean α value on 1 June is almost double to that on 13 July. It is known that the spectral variation of Angstrom exponent (α) is strongly dependent on the atmospheric turbidity (β) and aerosol type [*Eck et al.*, 1999; *Cachorro et al.*, 2001; *Reid et al.*, 1999]. The backward trajectories for the two respective days indicated the presence of transport of a significant fraction of fine-mode (nucleation and accumulation) aerosol from the central and northern parts of the Indo-Gangetic basin (1 June) leading to the increase in columnar burden in the shorter wavelength, while the transport of coarse mode

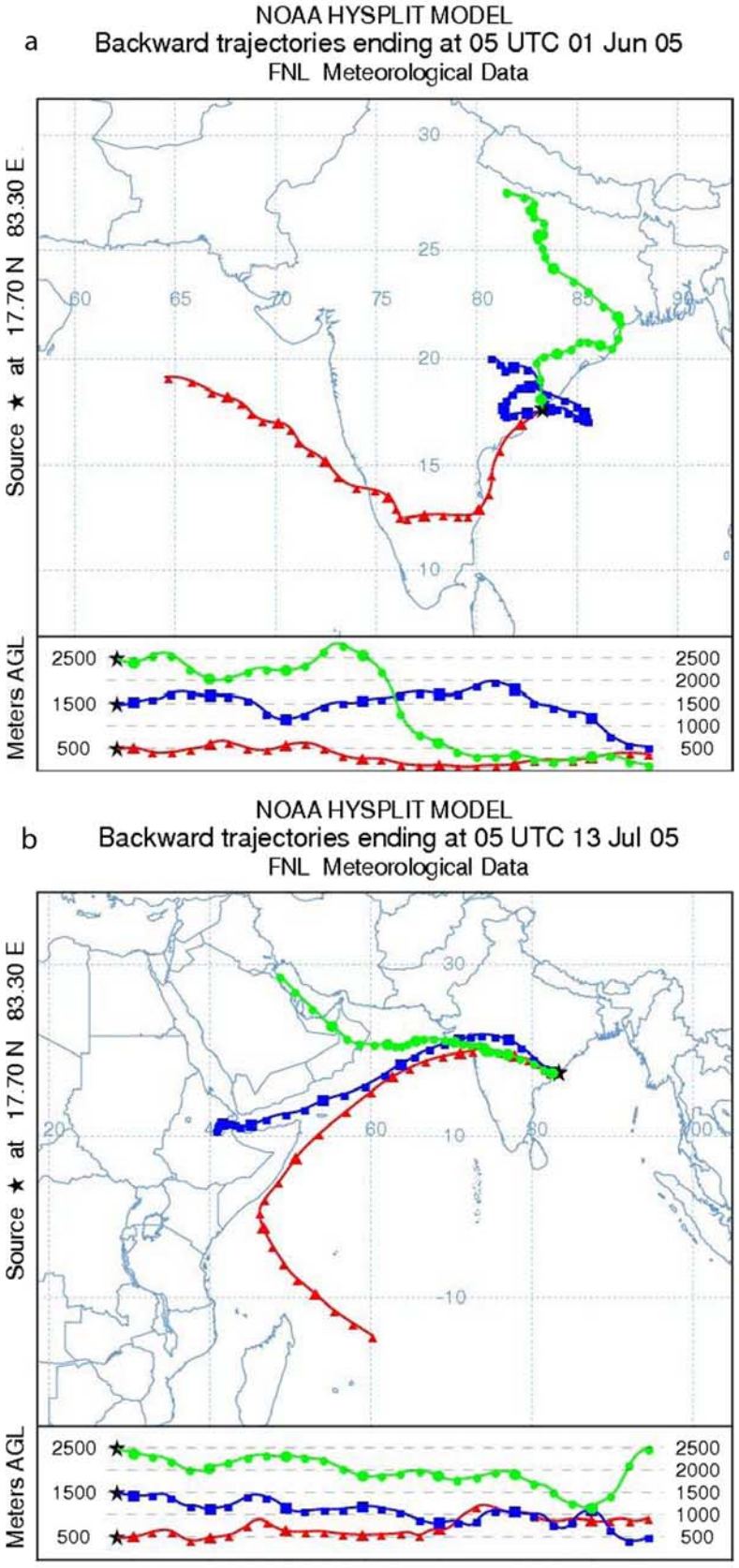

Figure 5. (a) HYSPLIT 7-day back trajectories showing the air mass pathways from central and northern India (1 June) when columnar fine-mode fraction dominated. (b) HYSPLIT 7-day back trajectories showing the air mass pathways from Arabian region (13 July) when Angstrom exponent α value was relatively lower.

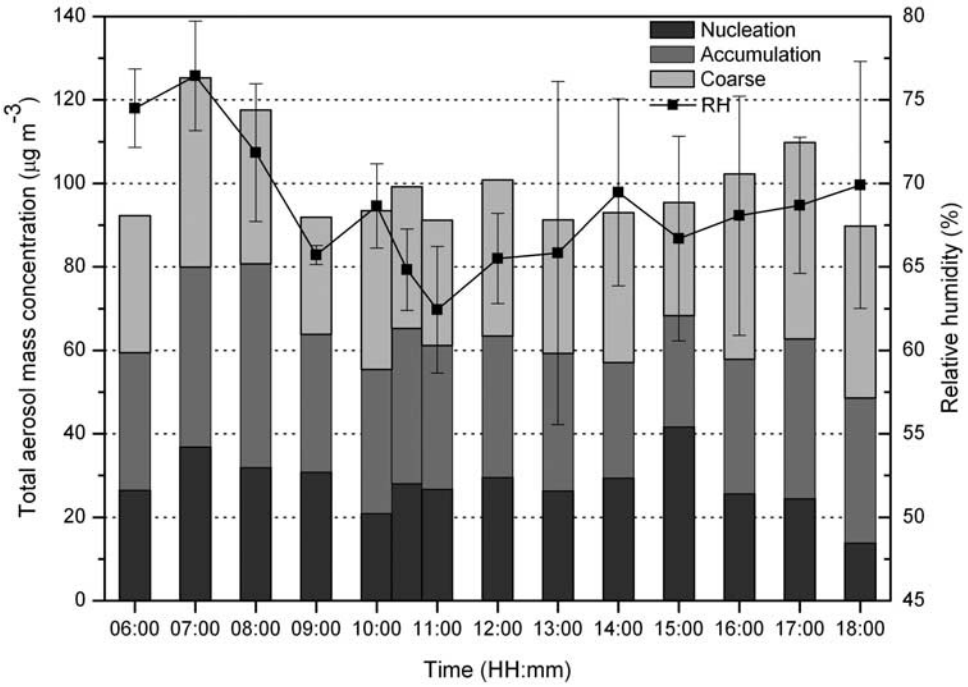

Figure 6. Diurnal variation of hourly mean total size-segregated near-surface aerosol mass concentration (μg m^{-3}) and relative humidity (%).

aerosol from Arabia/African countries (13 July) indicated that the coarser dust particles carried away by the wind ($\sim$5 ms^{-1}) were added to the column along with the localized aerosol, leading to the high AOD at longer wavelengths. Also, the Angstrom turbidity coefficient (β; AOD at 1 μm) value on 1 June and 13 July were found to be 0.18 (low) and 1.15 (high), which further indicates that the aerosol columnar mass loading on 13 July was dominated by coarse mode while that on 1 June was of fine-mode dominance.

4.3. Near-Surface Aerosol Mass Concentration

[19] Size-segregated aerosol mass concentrations in 10 different size bins measured using QCM have been classified into three categories, namely, coarse mode particles with size ranging between 1 and 10 μm (total mass collected in stages 2, 3 and 4 of QCM), accumulation mode particles in the size range 0.1 to 1 μm (total mass collected in stages 5, 6, 7 and 8) and the nucleation mode particles with size less than 0.1 μm (total mass collected in stages 9 and 10). Aerosol mass obtained from stage 1 of the QCM device is excluded in the classification as it integrates all particles of size greater than 12.5 μm and no meaningful mean radius could be assigned to this stage. The aerosol particles collected in the stage 1 are either sea-salt particles produced by breaking of sea waves or wind blown coarse particles reaching from the surrounding landmasses. Since the particles collected in this stage are bigger in size, most of the time the total mass measured in this stage is very high. Mass concentration for the particles collected in the first stage of QCM and the coarse mode depend on the surface-level wind speed and relative humidity of the ambient atmosphere.

[20] The near-surface aerosol mass concentration is highly dynamic and shows variation with time of the day owing to the influence of mesoscale processes. They respond distinctly to mesoscale land/sea breeze circulations and perceptibly to the changes in Atmospheric Boundary Layer (ABL) dynamics. Figure 6 shows the mean hourly diurnal variation of the total aerosol mode concentration with RH during the period of our observation. It was observed that two prominent peaks of near-surface concentrations in the morning ($\sim$0700 IST) and in the evening ($\sim$1700 IST) are due to the short-lived enhancement in total mass concentration occurring during the periods around the breeze reversals and thus can be attributed to the horizontal convergence of aerosols in the boundary layer. In addition to the horizontal convergence, the morning rise in the boundary layer inversion, owing to heating of the land by solar insolation which breaks the low-level stable layers and the resulting turbulence bring in the aerosols in the entrainment zone owing to the so-called fumigation effect [*Stull*, 1988]. This leads to a small increase in the concentration shortly after sunrise (as seen from Figure 6). On sunrise, the continuous heating of Earth's surface by the solar radiation results in thermal mixing in the ABL and consequently ABL depth increases steadily till it attains a maximum in the afternoon hours ($\sim$1200 IST). Late in the evening and through out the night, weak wind and the radiative cooling of the ground surface results in the suppression or weakening of turbulent mixing and consequently in the shrinking of ABL depth.

[21] During daytime the dispersion of aerosols will be high owing to the large ventilation coefficient (defined as the product of mixing height and horizontal wind speed) and thus the concentration remained less. On the basis of the observations using low-altitude wind profilers measurements at a nearby tropical Indian station, Gadanki (13.5°N, 79.2°E), a low value of ventilation coefficient was reported

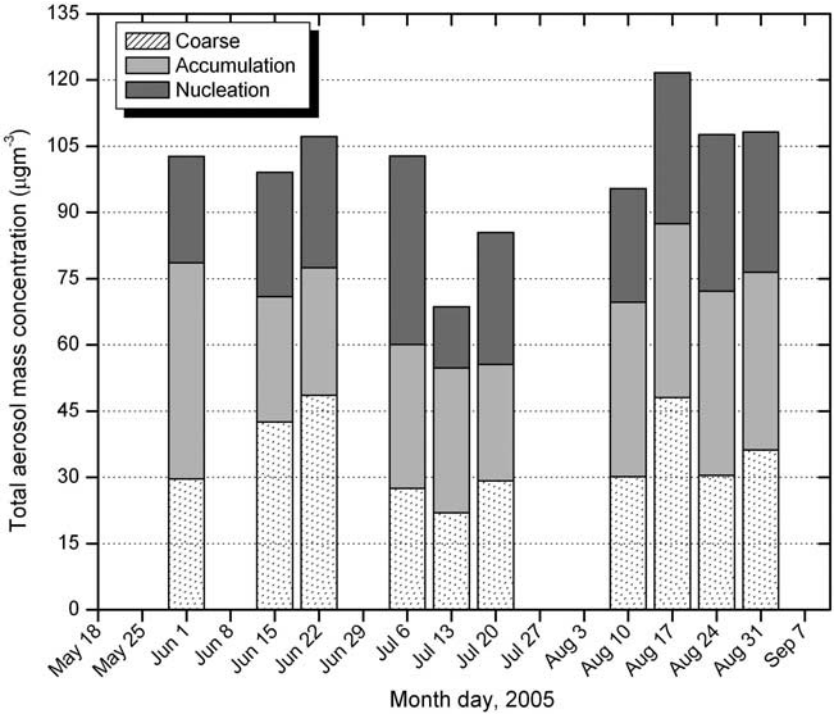

Figure 7. Time series of the average total surface-level aerosol mass concentration (M_{QCM} given in $\mu g\ m^{-3}$) during the period of our study (June–August 2005).

during early morning and late night hours and high values during daytime [*Krishnan and Kunhikrishnan*, 2002]. In another study over Gadanki, *Krishnan and Kunhikrishnan* [2004] observed the ABL height to become maximum during premonsoon period and minimum during dry months. Hence, the observation of morning peak is due to the combined effect of fumigation and horizontal convergence of opposing breezes and the evening peak to the shallow boundary layer and the reduced ventilation coefficient. Thus the diurnal variation of aerosol surface mass concentration depends on the combination of the strength of particulate sources, the local wind and the degree of natural ventilation available. In the mean diurnal variation for the summer monsoon period of 2005 it was observed that the coarse mode and accumulation mode aerosol concentrations correlated with the RH at 0.41 and 0.48 respectively, while the nucleation mode has a negligible correlation of 0.09. The nucleation and accumulation aerosol in total contributed 63% to the total daily aerosol mass concentration while the coarse mode aerosols contributed 37% when observed individually. During continental air mass period, the accumulation and fine size range dominate while during marine air mass period it is coarse and large particles that dominate. The increase in aerosol mass concentration in the supermicron range/coarse mode during marine air mass period can also partly be due to the increase in relative humidity or reduction in temperature during this period. Thus an increase in the large particle mode marks the usual hygroscopic growth indicating the clear resemblance of the association of β with the coarse mode aerosol loading.

[22] Figure 7 shows the temporal variation of total aerosol mass concentration during the period of observation. Total aerosol mass concentration during this period varied from 95 to 128 $\mu g/m^3$ with a monthly mean of 114 ± 15 $\mu g/m^3$. The accumulation mode aerosols produced by the condensation growth and coagulation of nucleation mode aerosols contribute maximum to PM10 mass. The aerosol mode concentration during this period varied from: 21 to 49 $\mu g/m^3$ (coarse), 26 to 49 $\mu g/m^3$ (accumulation), and 13 to 36 $\mu g/m^3$ (nucleation). The presence of fine-mode aerosol transport at high altitudes (<3 km) on 1 June well correlated with the high surface aerosol fine-mode fraction while the presence of dust transport on 13 July at the same altitudes has no enhancement on the surface coarse mode aerosol concentration. Hence, the presence of high-altitude long-range aerosol transport from distinct sources have associated signatures at the surface-level fine-mode aerosol concentration while that of coarse mode aerosol have no tracers even though there are traces of the transport of dust from Africa/Arabian regions. Although, during the monsoon season, occasional spells of rain kept the surface damp and uncertainty of loose soil being lifted by the wind prevailed, the locally produced dust/sea spray contributed for the high values of coarse mode aerosol mass. Occasional low values of coarse mode aerosols result owing to inefficient lifting mechanisms and enrichment in surface resistance features.

4.4. Relation Between Columnar and Surface-Level Aerosol Characteristics

[23] In order to investigate the correlation between the columnar and surface-level aerosol characteristics, we tried to establish a linear regression relation between the values of Angstrom wavelength exponent (α) and aerosol mass concentration measurements. The continental aerosols of mainly anthropogenic origin lie in the accumulation regime (0.1–1.0 μm), while wind blown dust and sea spray aerosols lie in the coarse regime (>1.0 μm). Soot from biomass burning and vehicular exhaust also lies in the

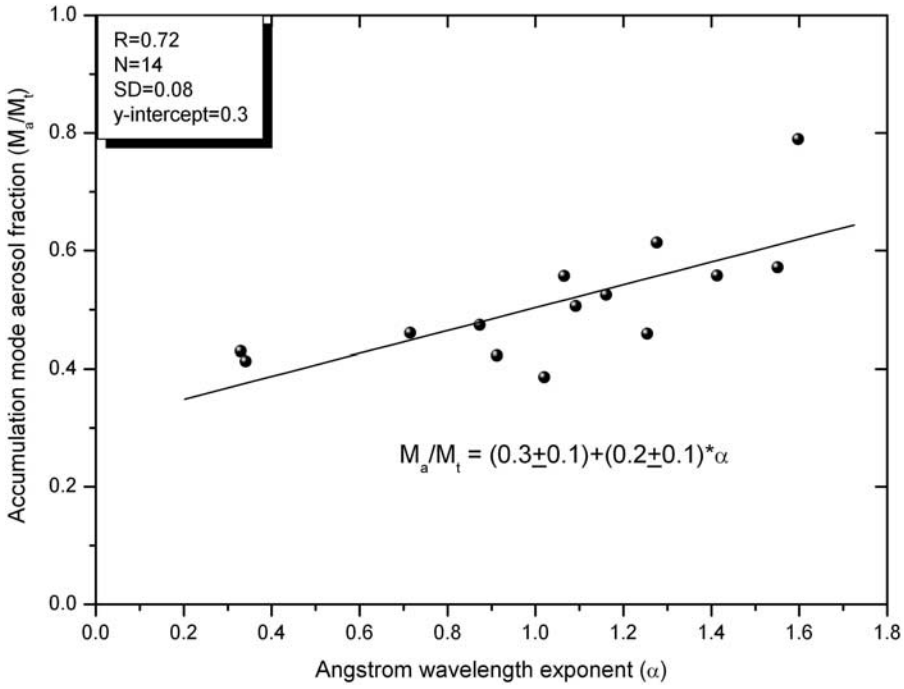

Figure 8. Scatterplot of M_a/M_t along with Angstrom wavelength exponent (α) for the days of simultaneous observations.

accumulation regime, which are long-lived and more amenable for long-distance transport while coarse mode particles having short life times are only of local relevance. Figure 8 shows the scatterplot between accumulation mode fraction (M_a/M_t) and Angstrom wavelength exponent (α). Here M_t and M_a denote the total aerosol mass concentration in the size range 0.05 to 25 μm in unit volume of ambient air and its respective accumulation mode concentration estimated from QCM measurements respectively. The observed scatterplot is due to the aerosol mass concentration values present within the relatively well mixed atmospheric boundary layer (ABL), where as the wavelength exponent values include not only the contribution from aerosols present with in the ABL but also those lying in the free troposphere, immediately above it. Relative contribution from these two regions is dependent on the extent of vertical mixing between them, which in turn depends on other meteorological conditions. It is observed that the near-surface aerosol accumulation mode fraction showed a high positive correlation of 0.75 while the surface aerosol coarse mode indicated a negative correlation of 0.28 with the Angstrom wavelength exponent (α). This might have been due to the efficient vertical transport of continental aerosols in this season and also the presence of an effective exchange between the mixed layer and free troposphere, thereby resulting in a better vertical homogeneity in their properties. The smaller particles with less inertia and larger surface area (for a given mass) are more influenced by these buoyant forces and become distributed in the column while the larger particles, on the other hand, will be more confined to lower heights.

4.5. Intercomparison of Surface Mass Concentrations

[24] Before presenting the composite picture of water-soluble ionic species in the aerosol samples collected using HVS, it is essential to examine the reliability, consistency and interchangeability of the measurements made by the QCM. The total mass concentration (M_{QCM}) and the total suspended particulate matter (M_{HVS} or TSP) obtained from HVS under nearly identical condition for the same duration of instrumental operation were shown in a scattered plot Figure 9. Here the M_{QCM} represents the measurements made using QCM with time weighted for the duration for which the HVS was operated. This means that

$$M_{QCM} = \left[\sum_{i=1}^{n} M_{ti}\Delta t_i \Big/ \sum_{i=1}^{n} \Delta t_i\right]$$

where Δt is the time interval between successive sampling at our location during which the total mass concentration is M_{ti} and n is the total number of samples during the period for which HVS was operated. A general agreement is observed despite the differences in the cut off diameters (the HVS has no upper cutoff size whereas QCM collects particles below 25 μm diameter) as the two instruments were operated at the same location. This indicates that the data can be mixed together fairly compositely to build the spatial composite. The QCM derived total aerosol mass concentration (M_{QCM}) and the HVS derived total particulate matter (TSP or M_{TSP}) fairly correlated with 0.78 during the period of simultaneous measurements from these instruments.

4.6. Aerosol Chemical Composition

[25] Aerosols produced from different natural and anthropogenic activities are mixed together and hence each aerosol particle is a composite of different chemical constituents. Chemical composition of aerosols determines their complex (contains real and imaginary parts) refractive

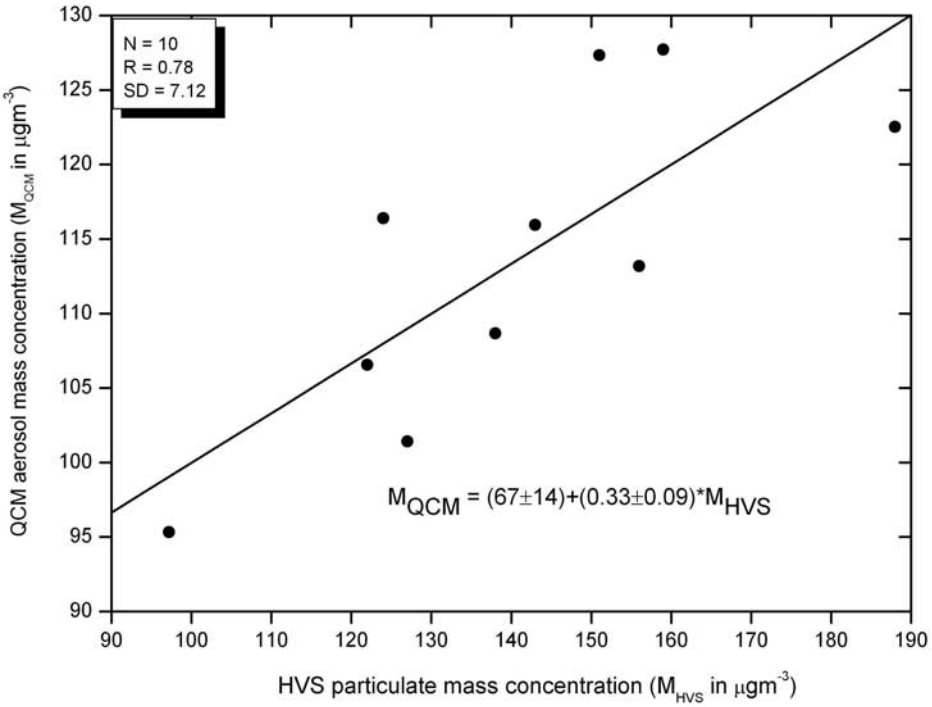

Figure 9. Scatterplot of QCM measured total aerosol mass concentration (μg m^{-3}) along with the HVS measured aerosol particulate mass concentration (μg m^{-3}).

index. Particle refractive index is an important parameter while determining the radiative effects. Information about the aerosol chemical composition covering all seasons and the spatial extent is virtually nonexistent over an east coast location, Visakhapatnam. In an attempt to characterize the aerosols over the location, we have started a systematic ambient aerosol sampling using high volume sampler (HVS). The major aerosol species found are sulphate, ammonium, nitrate, sea salt (Na and Cl), soot, dust (Mg, Mn, Fe, Co, Ni, and Cu) and organics. The collected aerosol samples during May–August 2005 were analyzed for various water-soluble ionic species (cations: NH_4^+, Na^+, K^+, Mg^{2+}, Ca^{2+}; anions: Cl^-, NO_3^-, SO_4^{2-} and HCO_3^-). During the period of observation it was observed that the total aerosol loading varied from 97 to 188 μg/m^3 with a mean of 143 ± 24 μg/m^3. In this, the water-soluble ionic species constituted an average of 46 ± 15 μg/m^3. Figure 10 represents the average percent contribution of water-soluble ionic species during May–August 2005. It was observed that the water-soluble fraction over Visakhapatnam during this period (southwest monsoon season) is mainly dominated by chloride (27.8%), sulphate (24.1%), sodium (20.9%), nitrate (8.9%), calcium (7%), bicarbonate (6.8%); and other trace ions (Mg^{2+}: 2.9%, K^+: 1.5% and NH_4^+: 0.2%) in minor concentrations. *Rastogi and Sarin* [2005] indicated from their long-term characterization of ionic species in aerosols over Ahmedabad that during southwest monsoon period (May–August), the contribution of Na^+ and Cl^- are significantly enhanced by 67% and 75% while the contributions from SO_4^{2-} and NO_3^- showed a decreasing trend by 18% and 55% respectively, than those observed during dry periods. It is observed that the water-soluble ionic species mainly Na^+, Mg^{2+}, Cl^-, NO_3^- and SO_4^{2-} showed a fourfold increase while HCO_3^- reduced to half the concentrations over Visakhapatnam during summer monsoon period when compared to those in Ahmedabad (23.0°N, 72.6°E, 49 m asl), an urban location in the semiarid region of western India.

4.6.1. Ion Balance

[26] Electrical charge balances of the observed ionic aerosol components are a useful tool to test the accuracy of measurements and to judge on the missing anions or cations. The charge balance between total cations (Σ^+) and total anions (Σ^-) measured in the water extracts of aerosols is shown in Figure 11. The mean measurement uncertainty is ~2.8 for the sum of anions (Cl^-, NO_3^-, SO_4^{2-} and HCO_3^-) and ~1.2 for the sum of cations (NH_4^+, Na^+, K^+, Mg^{2+},

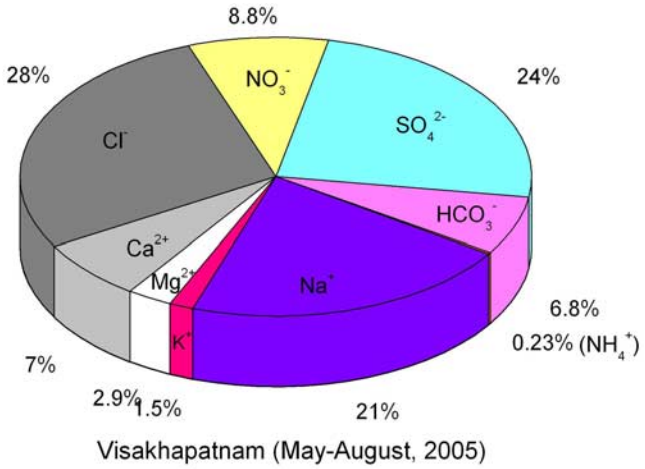

Figure 10. Mean percent contribution of water-soluble ionic species in aerosols over Visakhapatnam during our period of study (May–August 2005).

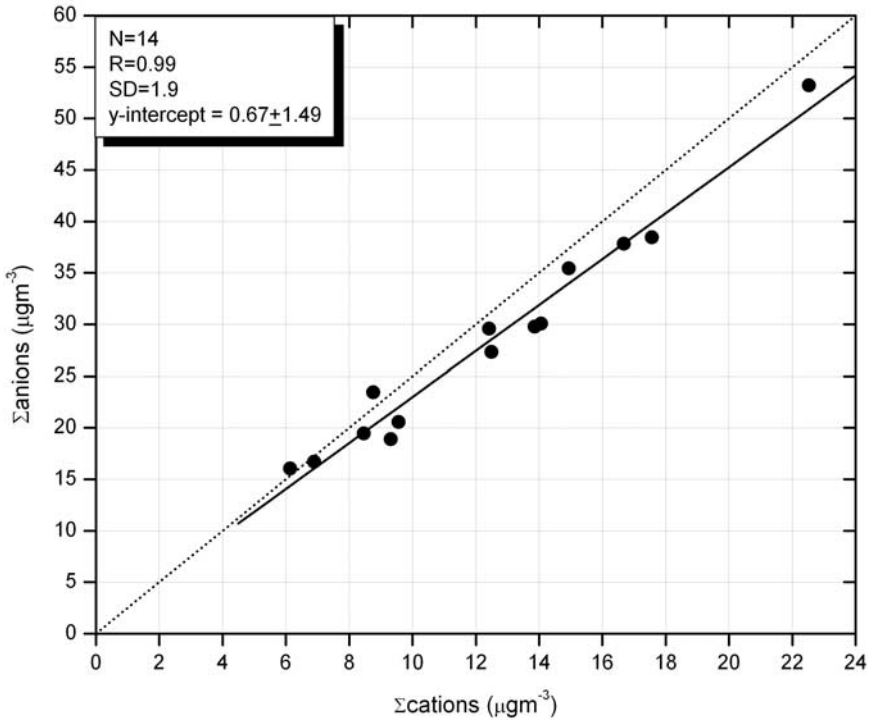

Figure 11. Ion balance between Σ cations and Σ anions representing quantitative characterization of water-soluble ionic species in aerosols during May–August 2005.

Ca^{2+}). The median of cation/anion ratio is now 0.44 strengthening the hypothesis that additional cations are necessary to balance aerosol anion charges. This significant shift was primarily caused by the deficiency of K^+ in the fine-mode aerosols, which is directly emitted by biomass fires and vegetation in this region. The Σ^+/Σ^- ratio vary from 0.37 to 0.49 with a mean and standard deviation of 0.44 ± 0.03 indicating that the samples show a noticeable cation deficit over the coastal urban location Visakhapatnam during this period. Earlier studies from the Indian region [*Kulshrestha et al.*, 1998; *Momin et al.*, 1999; *Venkataraman et al.*, 2002] have reported the cation excess in ion balance of water extracts attributing largely to the lack of bicarbonate measurements. Measurement of total carbonate content provides the maximum neutralization capacity of the aerosols while the water-soluble fraction provides the actual chemical neutralization occurring in the atmosphere. The mean uncertainty is ~1.23 for the sum of anions and ~0.05 for NH_4^+. Ammonia is mostly emitted by combustion processes, volatilization from manure and fertilizer application, plays a key role in neutralizing acidic atmospheric compounds [*Asman et al.*, 1998]. Owing to heterogeneous reactions involving gaseous NH_3 as well as sulphur dioxide (SO_2), nonvolatile aerosol constituents like $(NH_4)_2SO_4$ and NH_4HSO_4 can be formed. Table 2 indicates the correlation matrix of several water-soluble ionic species in aerosols. Initially, the NH_4^+ showed a negative correlation with all the other water-soluble ionic species owing to sudden rise in concentrations by 1.5 times during August. Excluding these concentration values, NH_4^+ showed a positive correlation varying from 0.04 to 0.59 with the various water-soluble ionic species. It is to be noted that sodium (Na^+), potassium (K^+), magnesium (Mg^{2+}) and chloride (Cl^-) have a perfect correlation (>0.79) among each other indicating the abun-

Table 2. Correlation Coefficients Matrix of Various Water-Soluble Ionic Species During the Summer Monsoon Season of 2005[a]

	NH_4^+	Na^+	K^+	Mg^{2+}	Ca^{2+}	Cl^-	NO_3^-	SO_4^{2-}	HCO_3^-	nss K^+	nss Mg^{2+}	nss Ca^{2+}	nss SO_4^{2-}
NH_4^+	1												
Na^+	0.236*	1											
K^+	0.068	0.802	1										
Mg^{2+}	0.268*	0.993	0.809	1									
Ca^{2+}	0.138	0.606	0.629	0.672	1								
Cl^-	0.085*	0.979	0.791	0.966	0.659	1							
NO_3^-	0.176	0.352	0.393	0.403	0.658	0.350	1						
SO_4^{2-}	0.415	0.474	0.681	0.548	0.622	0.391	0.567	1					
HCO_3^-	0.041*	0.731	0.700	0.725	0.564	0.773	0.084	0.286	1				
nss K^+	0.516	-	0.294	-	-	-	0.027	0.177	-	1			
nss Mg^{2+}	0.524	-	0.222	0.050	0.563	-	0.435	0.634	-	0.394	1		
nss Ca^{2+}	0.231	0.457	0.535	0.533	0.985	0.521	0.658	0.591	0.469	0.070	0.644	1	
nss SO_4^{2-}	0.618	0.105	0.395	0.192	0.442	0.020	0.489	0.925	0.008	0.383	0.745	0.471	1

[a]Dashes indicate negative correlation; asterisks indicate negative correlation without eliminating the August (2005) month values of ammonium ion concentration.

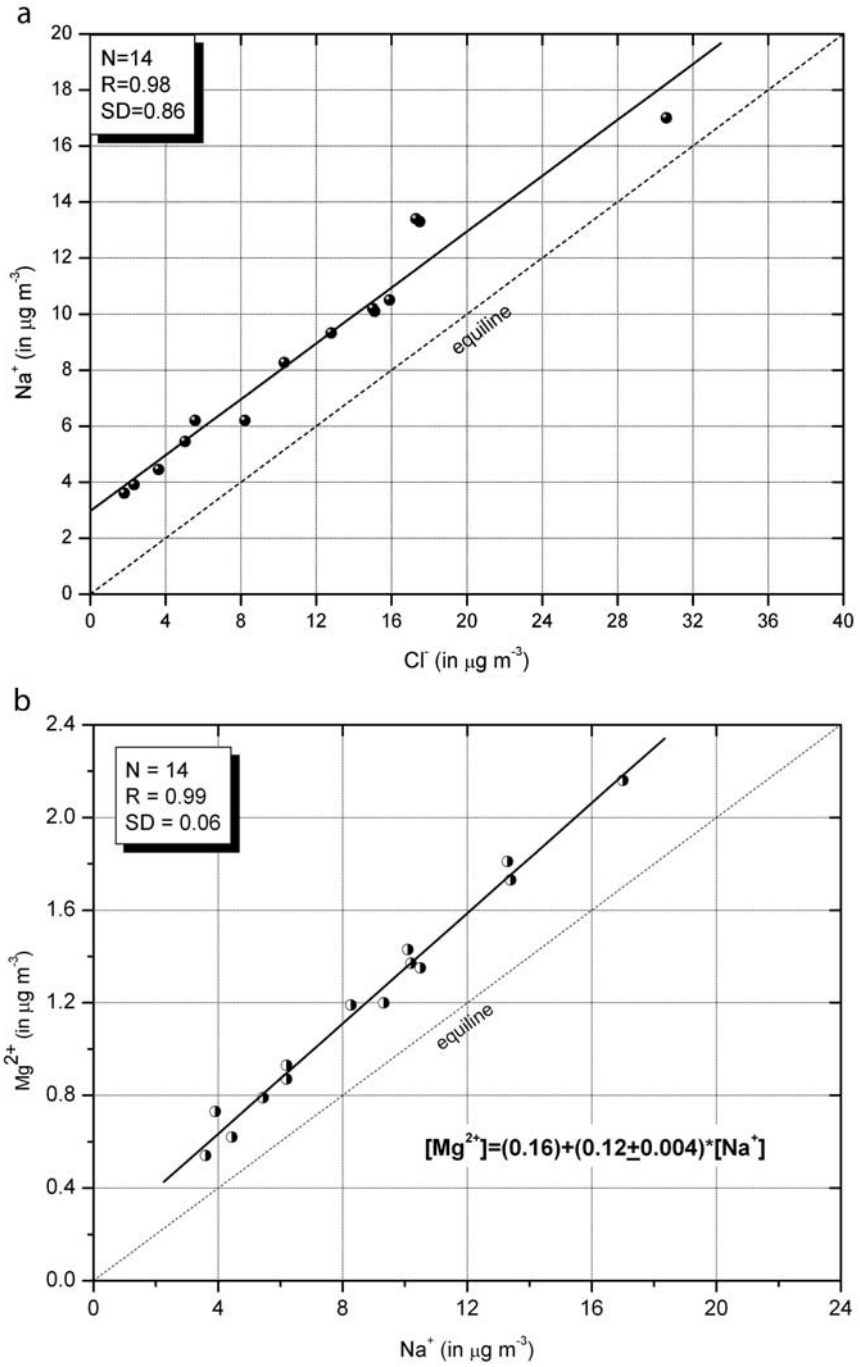

Figure 12. (a) Scatterplot for Na^+ and Cl^- with respect to equiline (or seawater line), suggesting that Na^+ and Cl^- are derived from sea salts. (b) Scatterplot for Mg^{2+} and Cl^- with respect to equiline, suggesting that a significant fraction of Mg^{2+} are derived from sea salts. The y-intercept indicates nss-Mg^{2+} concentration (μg m^{-3}).

dance of sea-salt aerosols and they alone contributed to about 53% of the total water-soluble ionic species in aerosols during this period.

4.6.2. Sea-Salt Aerosol

[27] Sea-salt aerosols are generated by various physical processes, especially the bursting of entrained air bubbles during whitecap formation [*Blanchard*, 1983; *Monahan et al.*, 1986], resulting in a strong dependence on wind speed. The higher loadings of sodium and chloride during this period can be attributed to the presence of sea-salt particles owing to high wind speeds (>5 ms^{-1}). Both sodium and chloride together contributed 48.7% of the total water-soluble fraction in this period. This aerosol may be the dominant contributor to both light scattering and cloud nuclei in those regions of the marine atmosphere where wind speeds are high and/or other aerosol sources are weak [*Quinn et al.*, 1998; *O'Dowd et al.*, 1997; *Murphy et al.*, 1998]. Sea-salt particles cover a wide size range

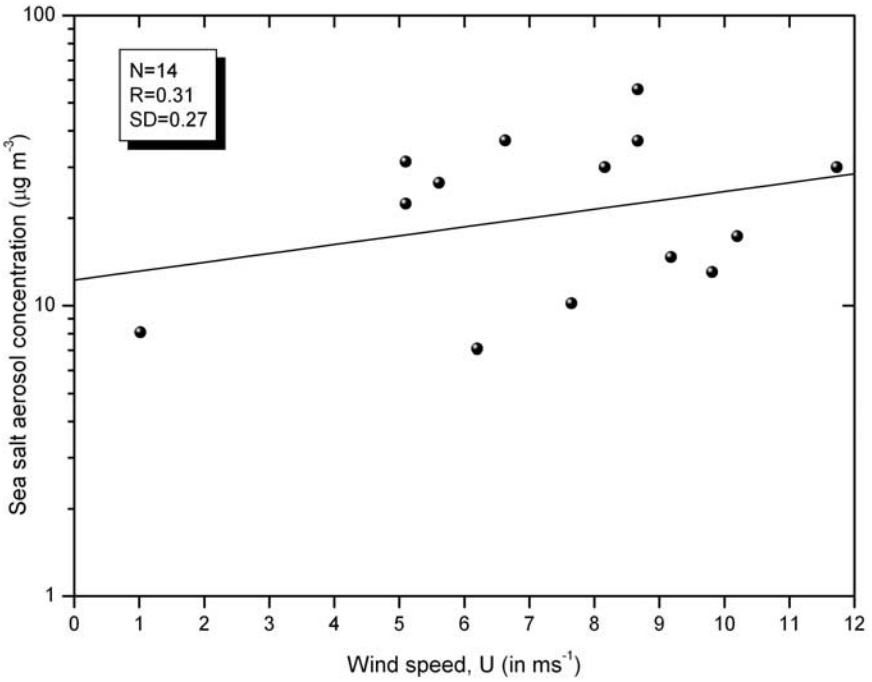

Figure 13. Dependence of sea-salt aerosol mass concentration (μg m^{-3}) on the prevailing wind speed (ms^{-1}) over Visakhapatnam during the summer monsoon season (May–August 2005).

(0.05–10 μm diameter), and have a correspondingly wide range of atmospheric lifetimes. Thus they act as very efficient cloud condensation nuclei (CCN), and therefore characterization of their surface production is of major importance for aerosol indirect effects. Sea-salt aerosol concentrations were calculated as:

$$\text{sea salt } (\mu\text{g m}^{-3}) = Cl^{-}(\mu\text{g m}^{-3}) + Na^{+}(\mu\text{g m}^{-3}) \times 1.47$$

where 1.47 is the seawater ratio of ($Na^+ + K^+ + Mg^{+2} + Ca^{+2} + SO_4^{2-} + HCO_3^-$)/$Na^+$ [*Holland*, 1978]. This approach prevents the inclusion of non-sea-salt K^+, Mg^{+2}, Ca^{+2}, SO_4^{2-}, and HCO_3^- in the sea-salt mass and allows for the loss of Cl^- mass through Cl^- depletion processes. It also assumes that all measured Na^+ is derived from seawater. Now calculating the sea-salt concentrations using the observed values of Na^+ and Cl^- concentrations, it was observed a variation from 7 to 56 μg/m^3 with a mean and standard deviation of 24 ± 14 μg/m^3 over Visakhapatnam during this period. The scatterplots among water-soluble ionic species were used to assess their major sources. Figures 12a and 12b show scatterplots for Na^+, Cl^- and Mg^{2+} with respect to equiline indicating that Na^+, Cl^- and a significant fraction of Mg^{2+} are derived from sea salts. The marginal excess of Cl^- over Na^+ could arise owing to the depletion of Na^+ as result of its reaction with other species or its additional source from local dust particles with disproportionate Cl^-/Na^+ ratio than in sea salts. For Mg^{2+} to become excess over Na^+, additional contribution of Mg^{2+} from regional mineral dust is required which can be found mainly during dry season.

[28] The dependence of sea-salt aerosol concentration on wind speed can be expressed as: $M = a\exp(bU)$, where M is the concentration of aerosol mass (μg/m^3) at wind speed U (ms^{-1}), b is a coefficient called 'wind index' (sm^{-1}) and a is the background aerosol mass concentration when the wind speed reaches zero [*Moorthy et al.*, 1997]. An increase in aerosol concentration with increase in wind speed was experimentally shown by *Woodcock* [1953] and later on by several researchers, *Lovett* [1978], *Exton et al.* [1985] and *O'Dowd and Smith* [1993]. The value of the coefficient a and b estimated for the aerosols collected in stage 1 of QCM during the present period are 19.57 and 0.03, respectively. The corresponding values reported by *Exton et al.* [1985] for North Atlantic Ocean are 14.30 and 0.17. Figure 13 shows the dependence of sea-salt aerosol concentration on the surface wind speed. Here the low value of r (=0.31) indicates importance of factors other than local wind speed in determining the sea-salt mass concentration, which include long-range transport and vertical mixing [*Quinn et al.*, 1998; *Bates et al.*, 1998]. The wind index for sea-salt aerosol concentration was obtained as 0.03 while the wind index for Na^+ and Cl^- concentrations was obtained as 0.06 and 0.12 respectively. The coefficient b does not depend on the season but depends on the wavelength; b = 0.12 for λ = 0.5 μm and b = 0.18 for λ = 1.02 μm [*Moorthy et al.*, 1997]. At a marine location where major part is contributed by sea salt, an increase in sea-salt contribution on the Angstrom parameter (α) is nearly at the same rate. Increased sea-salt aerosols (SSA) raise the single scattering albedo and increase the optical depth. Higher single scattering albedo decreases the surface forcing efficiency, while greater optical depths increase forcing [*Podgorny et al.*, 2000]. Since the production of aerosol species other than sea salt does not depend on wind speed, the enhancement of AOD with increased surface wind speed is attributed to the local production of sea-salt aerosols.

4.6.3. Non-Sea-Salt Aerosols

[29] The temporal variation of SO_4^{2-} and NH_4^+ ions follow each other closely, indicating that some $(NH_4)_2SO_4$ and/or

NH_4HSO_4 probably are present in the fine particles. Usually Cl^- and NO_3^- are found in relatively small amounts, principally in the 1.0–1.8 μm aerodynamic diameter range. While the Cl^- indicates the presence of sea salt, the NO_3^- in particle sizes >1 μm specifies that a small amount of sea salt has been in some cases partly transformed by atmospheric chemical reactions to produce sodium nitrate ($NaNO_3$). Since chloride can be displaced from aerosol by reaction with sulphuric or nitric acid, chloride concentrations alone do not permit an accurate assessment of the sea salt present.

[30] Using Na^+ as a reference element for sea-salt correction [*Keene et al.*, 1986], the non-sea-salt component has been calculated for K^+: 48%, Mg^{2+}: 13%, Ca^{2+}: 89% and SO_4^{2-}: 78% representing the period under study. A correlation coefficient of 0.47 for nss-Ca^{2+} and HCO_3^- indicates the presence of sources of mineral dust. The y-intercept obtained by the linear fit for Mg^{2+} versus Na^+ indicates the presence of non-sea-salt component of magnesium in aerosol species (as shown in Figure 12). Next to sea-salt aerosols, about 33% of the total water-soluble ionic species concentration is from the anthropogenically derived components NO_3^- and SO_4^{2-}, which in turn chemically interact with the mineral aerosols. The major sources of NO_3^- and SO_4^{2-} in the atmosphere are the oxidation of their precursors NO_x and SO_2, respectively, emitted from various anthropogenic activities. Both NO_3^- and SO_4^{2-} are largely produced as secondary aerosols during the process of coal combustion, biomass burning and vehicular emissions [*Seinfeld and Pandis*, 1998]. Sulphate particles are hygroscopic and hence they accrete water vapor, especially above the so-called deliquescence point. The uptake of water implies that both the size distribution and refractive index change, thereby modifying the optical parameters. The nss-SO_4^{2-}/NO_3^- weight ratio varies from 1.1 to 2.9 with an average of 2.1 and standard deviation of 0.5, indicating of relative dominance by anthropogenic emissions of SO_2 and NO_x with gas to particulate phase conversions. Owing to anthropogenic emissions of SO_x and NO_x, both sulphate and nitrate aerosols respectively are formed via both gas and aqueous phase chemistry. A molar ratio of less than 1 for NH_4^+ to nss-SO_4^{2-} around 0.5 indicates a value typical for marine regions where there is insufficient NH_4^+ to fully neutralize the sulphate aerosol [*Quinn et al.*, 1988]. Smoke from biomass burning leads to a significant increase in cloud condensation nuclei (CCN) concentration causing alteration of cloud properties. Both, water-soluble inorganic aerosol species and soluble gases are expected to play a major role in the nucleation and growth of cloud droplets under polluted as well as under clean conditions.

5. Summary and Conclusions

[31] 1. Negative second-order Angstrom wavelength exponent (α^1) during postrainy days indicated the dominance of aerosol fine-mode fraction. These aerosols undergo transformation processes resulting in the increase of coarse mode aerosols during prerainy days as observed by the positive curvature of α^1 during the period of observation.

[32] 2. The nucleation and accumulation mode aerosols in total contributed 63% of the total daily aerosol mass concentration while the coarse mode alone contributed 37% implicating that the locally produced dust or sea-salt aerosols contributing for the higher values of coarse mode aerosols.

[33] 3. Columnar Angstrom wavelength exponent α showed a positive correlation of 0.72 with the near-surface accumulation mode fraction while the same indicated a negative correlation of 0.28 with aerosol coarse mode fraction.

[34] 4. Sodium (Na^+), potassium (K^+), magnesium (Mg^{2+}) and chloride (Cl^-) have a perfect correlation (>0.79) among each other indicating the abundance of sea-salt aerosols and they alone contributed to about 53% of the total water-soluble ionic species in aerosols during this period.

[35] 5. The cation/anion ratio varied from 0.37 to 0.49 with a mean and standard deviation of 0.44 ± 0.03 indicating that the samples showed a noticeable cation deficit over the coastal urban location Visakhapatnam during this period.

[36] 6. The water-soluble ionic species mainly Na^+, Mg^{2+}, Cl^-, NO_3^- and SO_4^{2-} showed a fourfold increase while HCO_3^- reduced to half the concentrations over Visakhapatnam during summer monsoon period when compared to those in Ahmedabad, an urban location in the semiarid region of western India.

[37] **Acknowledgments.** This work is supported by the Indian Space Research Organization, Geosphere-Biosphere Programme. The back trajectories were produced with HYSPLIT from the NOAA ARL Web site (available at http://www.arl.noaa.gov/ready/hysplit4.html/).

References

Angstrom, A. (1964), Technique of determining the turbidity of the atmosphere, *Tellus*, *13*, 214.

Asman, W. A. H., M. A. Sutton, and J. K. Schjorring (1998), Ammonia: Emission, atmospheric transport and deposition, *New Phytol.*, *139*(1), 27–48, doi:10.1046/j.1469-8137.1998.00180.x.

Bates, T. S., B. J. Huebert, J. L. Gras, F. B. Griffiths, and P. A. Durkee (1998), International Global Atmospheric Chemistry (IGAC) Project's First Aerosol Characterization Experiment (ACE 1), Overview, *J. Geophys. Res.*, *103*, 16,297–16,318, doi:10.1029/97JD03741.

Blanchard, D. C. (1983), *The Production, Distribution, and Bacterial Enrichment of the Sea-Salt Aerosol: The Air-Sea Exchange of Gases and Particles*, edited by P. S. Liss and W. G. N. Slinn, D. Reidel, pp. 407–454, Norwell, Mass.

Cachorro, V. E., R. Vergaz, and A. M. de Frutos (2001), A quantitative comparison of (-Angstrom turbidity parameter retrieved in different spectral ranges based on spectroradiometer solar radiation measurements, *Atmos. Environ.*, *35*, 5117–5124, doi:10.1016/S1352-2310(01)00321-1.

d'Almeida, G. A., P. Koepke, and E. P. Shettle (1991), *Atmospheric Aerosols: Global Climatology and Radiative Characteristics*, 559 pp., A. Deepak, Hampton, Va.

Delage, Y. (1974), A numerical study of the nocturnal atmospheric boundary layer, *Q. J. R. Meteorol. Soc.*, *100*, 351–364, doi:10.1002/qj.49710042507.

Eck, T. F., B. N. Holben, J. S. Reid, O. Dubovik, A. Smirnov, N. T. O'Neill, I. Slutsker, and S. Kinne (1999), Wavelength dependence of optical depth of biomass burning, urban and desert dust aerosol, *J. Geophys. Res.*, *104*, 31,333–31,349, doi:10.1029/1999JD900923.

Exton, H. J., J. Latham, P. M. Park, S. J. Perry, M. H. Smith, and R. R. Allan (1985), The production and dispersal of marine aerosol, *Q. J. R. Meteorol. Soc.*, *111*, 817–837, doi:10.1256/smsqj.46908.

Franke, K., A. Ansmann, D. Muller, D. Althausen, C. Venkataraman, M. S. Reddy, F. Wagner, and R. Scheele (2003), Optical properties of the Indo-Asian haze layer over the tropical Indian Ocean, *J. Geophys. Res.*, *108*(D2), 4059, doi:10.1029/2002JD002473.

Ganguly, D., A. Jayaraman, and H. Gadhavai (2006), Physical and optical properties of aerosols over an urban location in western India: Seasonal variabilities, *J. Geophys. Res.*, *111*, D24206, doi:10.1029/2006JD007392.

Gathman, S. G. (1983), Optical properties of the marine aerosol as predicted by the Navy aerosol model, *Opt. Eng.*, *22*, 57–62.

Hanel, G. (1976), The properties of atmospheric aerosol particles as function of relative humidity at the thermodynamic equilibrium with surrounding moist air, *Adv. Geophys.*, *19*, 73–188.

Holland, H. D. (1978), *The Chemistry of the Atmosphere and Oceans*, 154 pp., John Wiley, Hoboken, N. J.

Intergovernmental Panel on Climate Change (IPCC) (2001), *Climate Change 2001: The Scientific Basis, Contribution of Working Group I to the Third Assessment Report of the Intergovernmental Panel on Climate Change*, edited by J. T. Houghton et al., Cambridge Univ. Press, New York.

Kaskaoutis, D. G., and H. D. Kambezidis (2006), Investigation on the wavelength dependence of aerosol optical depth in the Athens area, *Q. J. R. Meteorol. Soc.*, *132*, 2217–2234, doi:10.1256/qj.05.183.

Keene, W. C., A. P. Pszenny, J. N. Galloway, and M. E. Hawley (1986), Sea-salt correction and interpretation of constituent ratios in marine precipitation, *J. Geophys. Res.*, *91*, 6647–6658, doi:10.1029/JD091iD06p06647.

Krishnan, P., and P. K. Kunhikrishnan (2002), A study on the effect of ventilation coefficient in the dispersion of pollutant over a tropical station, *Bull. IASTA*, *14*, 294–297.

Krishnan, P., and P. K. Kunhikrishnan (2004), Temporal variation of ventilation coefficient at a tropical station using UHF wind profiler, *Curr. Sci.*, *86*(3), 447–451.

Kulshrestha, U. C., A. Sexena, N. Kumar, K. M. Kumari, and S. S. Srivastava (1998), Chemical composition and association of size differentiated aerosols at a suburban site in a semi-arid tract of India, *J. Atmos. Chem.*, *29*, 109–118, doi:10.1023/A:1005796400044.

Lovett, R. F. (1978), Quantitative measurements of airborne sea-salt in the North Atlantic, *Tellus*, *30*, 358–363.

Momin, G. A., P. S. P. Rao, P. D. Safai, K. Ali, M. S. Naik, and A. D. Pillai (1999), Atmospheric aerosol characteristic studies at Pune and Thiruvananthapuram during INDOEX Programme 1998, *Curr. Sci.*, *76*, 985–989.

Monahan, E. C., D. E. Spiel, and K. L. Davidson (1986), A model of marine aerosol generation via whitecaps and wave disruption, in *Oceanic Whitecaps and Their Role in Air–Sea Exchange Processes*, edited by E. C. Monahan and G. M. Niocaill, pp. 167–174, D. Reidel, Norwell, Mass.

Moorthy, K. K., and S. K. Satheesh (2000), Characteristics of aerosols over remote island, Minicoy in the Arabian Sea: Optical properties and retrieved size characteristics, *Q. J. R. Meteorol. Soc.*, *126*, 81–109, doi:10.1256/smsqj.56204.

Moorthy, K. K., P. R. Nair, and B. V. Krishna Murthy (1991), Size distribution of coastal aerosols: Effects of local sources and sinks, *J. Appl. Meteorol.*, *30*, 844–852, doi:10.1175/1520-0450(1991)030<0844:SDOCAE>2.0.CO;2.

Moorthy, K. K., B. V. K. Murthy, and P. R. Nair (1993), Sea breeze front effects on boundary layer aerosols at a tropical coastal station, *J. Appl. Meteorol.*, *32*, 1196–1205, doi:10.1175/1520-0450(1993)032<1196:SBFEOB>2.0.CO;2.

Moorthy, K. K., S. K. Satheesh, and B. V. Krishna Murthy (1997), Investigations of marine aerosols over tropical Indian Ocean, *J. Geophys. Res.*, *102*, 18,827–18,842, doi:10.1029/97JD01121.

Morys, M., F. M. Mims III, S. Hagerup, S. E. Anderson, A. Baker, J. Kia, and T. Walkup (2001), Design calibration and performance of MICROTOPS II handheld ozone monitor and Sun photometer, *J. Geophys. Res.*, *106*, 14,573–14,582, doi:10.1029/2001JD900103.

Murphy, D. M., D. S. Thompson, and M. J. Mahoney (1998), In situ measurements of organics, meteoritic material, mercury, and other elements in aerosols at 5 to 19 kilometers, *Science*, *282*, 1664–1669, doi:10.1126/science.282.5394.1664.

Niranjan, K., B. Malleswara Rao, A. Saha, and K. S. R. Murthy (2004), Aerosol spectral optical depths and size characteristics at a coastal industrial location in India—Effect of synoptic and mesoscale weather, *Ann. Geophys.*, *22*, 1851–1860.

Niranjan, K., B. L. Madhavan, and V. Sreekanth (2007), Micro pulse Lidar observation of high-altitude aerosol layers at Visakhapatnam located on the east coast of India, *Geophys. Res. Lett.*, *34*, L03815, doi:10.1029/2006GL028199.

O'Dowd, C. D., and M. H. Smith (1993), Physicochemical properties of aerosols over the northeast Atlantic: Evidence for wind speed related submicron sea-salt aerosol production, *J. Geophys. Res.*, *98*, 1137–1149, doi:10.1029/92JD02302.

O'Dowd, C., M. H. Smith, I. E. Consterdine, and J. A. Lowe (1997), Marine aerosol, sea-salt, and the marine sulphur cycle: A short review, *Atmos. Environ.*, *31*, 73–80, doi:10.1016/S1352-2310(96)00106-9.

Pillai, P. S., and K. K. Moorthy (2001), Aerosol mass-size distribution at a tropical coastal environment: Response to mesoscale and synoptic processes, *Atmos. Environ.*, *35*, 4099–4112, doi:10.1016/S1352-2310(01)00211-4.

Podgorny, I. A., W. C. Conant, V. Ramanathan, and S. K. Satheesh (2000), Aerosol modulation of atmospheric and surface solar heating over the tropical Indian Ocean, *Tellus, Ser. B*, *52*, 947–958.

Prospero, J. M. (1979), Mineral sea-salt aerosol concentrations in various ocean regions, *J. Geophys. Res.*, *84*, 725–731, doi:10.1029/JC084iC02p00725.

Pruppacher, H. R., and J. D. Klett (1978), *Microphysics of Clouds and Precipitation*, pp. 193–195, D. Reidel, Norwell, Mass.

Quinn, P. K., R. J. Charlson, and T. S. Bates (1988), Simultaneous observations of ammonia in the atmosphere and ocean, *Nature*, *335*, 336–338, doi:10.1038/335336a0.

Quinn, P. K., D. J. Coffman, V. N. Kapustin, T. S. Bates, and D. S. Covert (1998), Aerosol optical properties in the marine boundary layer during the first Aerosol Characterization Experiment (ACE 1) and the underlying chemical and physical aerosol properties, *J. Geophys. Res.*, *103*, 16,547–16,563, doi:10.1029/97JD02345.

Rao, Y. P. (1976), *South West Monsoon*, *IMD Monogr.*, vol. 1, 367 pp., India Meteorol. Dep., Delhi.

Rastogi, N., and M. M. Sarin (2005), Chemical characteristics of individual rain events from a semi arid region in India: Three year study, *Atmos. Environ.*, *39*, 3313–3323, doi:10.1016/j.atmosenv.2005.01.053.

Reid, J. S., T. F. Eck, S. A. Christopher, P. V. Hobbs, and B. N. Holben (1999), Use of an Angstrom exponent to estimate the variability of optical and physical properties of aging smoke particles in Brazil, *J. Geophys. Res.*, *104*, 27,473–27,489, doi:10.1029/1999JD900833.

Roberts, G. C., P. Artaxo, J. Zhou, E. Swietlicki, and M. O. Andreae (2002), Sensitivity of CCN spectra on chemical and physical properties of aerosol: A case study from the Amazon Basin, *J. Geophys. Res.*, *107*(D20), 8070, doi:10.1029/2001JD000583.

Russell, P. B., et al. (1993), Pinatubo and pre-Pinatubo optical depth spectra: Mauna Loa measurements, comparisons, inferred particle size distribution, radiative effects and relationships to Lidar data, *J. Geophys. Res.*, *98*, 22,969–22,985, doi:10.1029/93JD02308.

Schuster, G. L., O. Dubovik, and B. N. Holben (2006), Angstrom exponent and bimodal aerosol size distributions, *J. Geophys. Res.*, *111*, D07207, doi:10.1029/2005JD006328.

Seinfeld, J. H., and S. N. Pandis (1998), *Atmospheric Chemistry and Physics: From Air Pollution to Climate Change*, John Wiley, Hoboken, N. J.

Sikka, D. R. (1980), Some aspects of large-scale fluctuations of summer monsoon rainfall over India in relation to fluctuations in planetary and regional scale circulation parameters, *Proc. Indian Acad. Sci. Earth Planet. Sci.*, *89*, 179–195.

Slater, J. F., and J. E. Dibb (2004), Relationships between surface and column aerosol radiative properties and air mass transport at a rural New England site, *J. Geophys. Res.*, *109*, D01303, doi:10.1029/2003JD003406.

Smirnov, A., A. Royer, N. T. O'Neill, and A. Tarussov (1994), A study of the link between synoptic air mass type and atmospheric optical parameters, *J. Geophys. Res.*, *99*, 20,967–20,982, doi:10.1029/94JD01719.

Smirnov, A., B. N. Holben, D. Savoie, J. M. Prospero, Y. J. Kaufman, and D. Tanre (2000), Relationship between column aerosol optical thickness and in situ ground based dust concentrations over Barbados, *Geophys. Res. Lett.*, *27*, 1643–1646, doi:10.1029/1999GL011336.

Stull, R. B. (1988), *An Introduction to Boundary Layer Meteorology*, Springer, New York.

Venkataraman, C., K. Reddy, S. Josson, and M. S. Reddy (2002), Aerosol size and chemical characteristics at Mumbai, India, during the INDOEX-IFP (1999), *Atmos. Environ.*, *36*, 1979–1991, doi:10.1016/S1352-2310(02)00167-X.

Vignati, E., G. de Leeuw, and R. Berkowicz (2001), Modeling coastal aerosol transport and effects of surf produced aerosols on process in the marine boundary layer, *J. Geophys. Res.*, *106*, 20,225–20,238, doi:10.1029/2000JD000025.

Woodcock, A. H. (1953), Salt nuclei in marine air as a function of altitude and wind force, *J. Meteorol.*, *10*, 362–371.

Zhang, X. Q., P. H. Mc Murry, S. V. Herring, and G. S. Casuccio (1993), Mixing characteristics and water content of submicron aerosols measured in Los Angeles and at the Grand Canyon, *Atmos. Environ. Part A*, *27*, 1593–1607.

B. L. Madhavan and K. Niranjan, Department of Physics, Andhra University, Visakhapatnam 530 003, India. (niranjankandula@hotmail.com)

M. M. Sarin and A. K. Sudheer, Physical Research Laboratory, Navrangpura, Ahmedabad 380 009, India.

V. Sreekanth, Space Physics Laboratory, Vikram Sarabhai Space Centre, Thiruvananthapuram 695 022, India.